1 **Microstructural investigation of the cooperative gelation of syndiotactic polystyrene and**

2 **high M$_W$ polyethylene glycol di-methyl ether in common solution in THF**

3

4 Fumitoshi Kaneko[1], Maria-Maddalena Schiavone[2], Hiroki Iwase[3], Shin-ichi Takata[4], Jürgen

5 Allgaier[5] and Aurel Radulescu[2*]

6

7 1 Graduate School of Science, Osaka University, 1-1 Machikaneyama, Toyonaka, Osaka

8 560-0043, Japan

9 2 Jülich Centre for Neutron Science (JCNS), Heinz Maier-Leibnitz Zentrum (MLZ),

10 Lichtenbergstrasse 1, 85748 Garching, Germany

11 3 Neutron Science and Technology Centre, Comprehensive Research Organization for

12 Science and Society CROSS, Tokai, 319-1106, Japan

13 4 Materials and Life Science Division, Japan Proton Accelerator Complex J-PARC, Tokai,

14 319-1195, Japan

15 5 Jülich Centre for Neutron Science (JCNS), Forschungszentrum Jülich GmbH, Jülich,

16 52425, Germany

17

18 Email: a.radulescu@fz-juelich.de

19

20 **Abstract**

21

22 The gelation of syndiotactic polystyrene (sPS) in THF in the presence of high molecular

23 weight PEGDME was investigated in detail using contrast-matching SANS complemented by

24 in situ FTIR. Using the contrast-matching method, the scattering contribution of each of the

25 two polymers in the common solution in THF at high temperature (110 °C), in the single-coil

26 conformational state and in the gelation state of sPS (below 40 °C and down to 10 °C) was

27 observed, and the structural characterization of the polymer coils and the junction structures

28 of the gel was obtained. The local scale conformation of the two types of polymer molecules

29 in the different regimes was additionally monitored by FTIR. The gelation and melting

30 temperatures were determined by DSC. sPS changes from the amorphous coil to the helical

31 TTGG conformation when the gelation temperature is passed, forming fibrillar morphologies

32 with a local 2D aspect due to cooperative interactions with the solvent molecules. These are

33 the junction structures of the large-scale network morphology of the gel. The high molecular

34 weight PEGDME transitions from the amorphous coil to an elongated amorphous

35 conformation and incorporates into the fibrillar morphology together with the sPS during the

36 gelation process. High M_W PEGDME alone in THF forms a "house of cards" gel consisting

37 of stacked lamellar structures on a smaller length scale, as shown by the scattering data. Thus,

38 in the presence of sPS, smaller and softer structures appear as a result of a cooperative

39 gelation process controlled by sPS. Incorporation of high M_W PEGDME into these aggregates

40 leads to polymer nanocomposites that can render the sPS hydrophilic, a topic that should be

41 the focus of future structural and morphological studies.

42

43

44 **Introduction**

45 Syndiotactic-polystyrene (sPS) is a relatively new material [1] that shows a complex

46 polymorphic behavior, including five different crystalline forms in which the chains adopt

47 either a planar zig-zag (α- and β-form) or a TTGG helical (γ-, δ- and ε-form) conformation

48 [2-4]. sPS is also able to form different kinds of co-crystalline (clathrate) phases with a large

49 number of small organic molecules which can be incorporated as guests in the cage- or

50 channels-like cavities between the polymer helices of the δ- and ε-forms, respectively [5-7].

51 Solvent-induced crystallization by using either the film casting from solution or the exposure

52 of amorphous films to solvents in vapor or liquid state leads to formation of helical co-

53 crystalline δ and ε forms, depending on the solvent type. Moreover, the initial guest

54 molecules in sPS co-crystals can be replaced smoothly with other kind of molecules by

55 exposure to vapors or liquid [8, 9]. The guest exchange procedure has the advantage to enable

56 sPS to form co-crystals even with chemical compounds that are difficult to incorporate into

57 the crystalline region by usual solution-cast and solvent-induced crystallization methods.

58 Following suitable guest extraction procedures emptied clathrate forms of s-PS (δ_e- or ε_e-

59 forms) may also be obtained, which correspond to pure helical form of s-PS free from the

60 guest molecules. The δ_e empty form is different from the γ-form, which is also a pure helical

61 form that is free of guest molecules, and is obtained either by annealing or heating the

62 clathrate δ form in the temperature range 110-170 °C, which purges away the solvent

63 molecules and yields closely packed helical chains in the crystal lattice [10]. The clathrate

64 forms are interesting for applications, when active guests can be incorporated in the sPS

65 films, leading to advanced materials for optical and magnetic applications [11-14], while the

66 emptied clathrates can find application as molecular sieves [15], for water purification from

67 chlorinated hydrocarbons.

68 It has been found that chemical compounds consisting of ethylene oxide repeat units

69 $(C_2H_4O)_n$ seem to possess sufficient affinity to become a guest of sPS co-crystals via guest

70 exchange procedure. This was confirmed in linear polyethylene glycols (PEGs) with

71 molecular weight (M_W) up to 1000 g/mol [16]. To answer the question of how such long-

72 chain compounds can be introduced into the crystalline cavities of the sPS lattice and what

73 conformation they adopt, it is desirable to obtain information on the general molecular shape

74 and local molecular structure of PEGs. This was elucidated in the case of the co-crystal

75 systems of sPS and short polyethylene glycol dimethyl ether (PEGDME) or triethylene-

76 glycol dimethyl ether (TEGDME) by a simultaneous experimental approach combining

77 measurements by small-angle neutron scattering (SANS) and Fourier-transform infrared

78 (FTIR) spectroscopy [17], with the film samples prepared by applying the guest exchange

79 procedure between the initial guest ($CHCl_3$) and the final guest (PEGDME or TEGDME).

80 However, although the guest exchange procedure is a useful method applicable for a variety

81 of chemical compounds, there is a practical problem for the co-crystallization of sPS with

82 PEG: the higher the molecular weight of the PEG guest, the longer the time required for this

83 procedure, which is attributable to a significant decrease in the diffusivity of PEG with

84 increasing molecular weight. Accordingly, it is unrealistic to adopt the guest exchange

85 procedure for the preparation of sPS co-crystals containing high-molecular weight PEG.

86 Recently it was found that sPS cocrystal films containing n-alkyl carboxylic acid (n-CA)

87 could be manufactured not only by applying the guest exchange procedure to sPS cocrystal

88 films but also by casting a chloroform ($CHCl_3$) solution containing two solutes, namely, the

89 host sPS and the guest n-CA [18]. Taking into account that solvent molecules are often

90 embraced in the crystalline region as guests when sPS films are prepared by casting from

91 solution, it is reasonable that a chemical species dissolved as a co-solute is taken into the

92 crystalline region if its affinity to the cavity of the sPS cocrystal lattice is larger than that of

93 the solvent molecule, as in the case of chemical compounds consisting of ethylene oxide

94 repeat units. Therefore, a new manufacturing process for sPS/PEG cocrystal film formation

95 was tested recently by casting binary solute solutions of the two components at different

96 weight ratios in $CHCl_3$ [19]. It was concluded that the procedure may be applicable PEG

97 with molecular weight as high as 20000 g/mol. According to previous studies [20] the PEG

98 molecules are distributed not only in the crystalline region but also in the amorphous region,

99 therefore in the case of high Mw PEG involved in the sample preparation it may be

100 considered that parts of the PEG chain may be included in the amorphous region.

101   On the other hand, the thermoreversible gelation of highly stereoregular polymers such as

102   sPS proceeds in two steps [21, 22]: a first step is an intramolecular coil-to-TTGG helix

103   transition by clustering of several chain segments or by organization of a single chains

104   segment, which is followed by an intermolecular association of multiple helix segments that

105   leads to the formation of the network structure. The gel properties depend on the structure of

106   the junction zones of starting gel. Depending on solvent type and/or thermal history, two

107   kinds of gels were reported, elastic gels that are characterized by helical chain conformation

108   and paste-like opaque gels characterized by trans-planar zigzag chain conformation.

109   Moreover, it was shown [23-26] that the characteristic shared by these thermoreversible gels

110   is the existence of fibre-like structures that seem to imply the absence of chain folding. sPS

111   would then produce fibrillar physical gels owing to helix stabilization by the solvent

112   molecules that suppresses chain folding and promotes formation of crystalline phase with

113   preferentially fibrillar morphology. It was also demonstrated by XRD [27, 28] and neutron

114   diffraction (ND) and SANS [24, 25] experiments that the structure of sPS fibrils in the gel

115   form is identical to that in the sPS δ co-crystalline phase (clathrates and intercalates).

116   Studies of gelation of s-PS in dichloroethane (DCE) in the presence of low M_W PEG

117   indicated that an increase of the PEG content in the gel led to change the structure of s-PS

118   from a helical conformation to a trans-zigzag one [29]. Another work has shown that when

119   PEG is dissolved along with the sPS in THF and sPS is allowed to undergo thermoreversible

120   gelation a PEG-rich solution formed separate domains inside the gel, of a size that is a

121   function of the concentration and M_W of PEG [30]. However, the interaction mechanism

122   between the sPS and high M_W PEG molecules in the transition from solution to gel state is

123   still a subject that requires further investigations.

124   In this work, we report the characterization of the physical gelation of sPS in the presence of

125   high molecular weight PEGDME from THF solution by contrast variation SANS. The choice

126   for PEGDME was to avoid clustering effects, which, as reported in [31], depend of the

127   polymer chain end groups. Formation and evolution of the structure and morphology at

128   different gelation temperatures in transition from the single-coil conformation of the two

129   polymer species at 110 °C to the ordered regular conformational of sPS in gel phase is

130   additionally characterized by FTIR analysis of the samples simultaneously with SANS. The

131   cooperative gelation process of sPS and high molecular weight PEGDME in common

132   solution in THF is discussed in a parallel analysis of the structure and morphology formed by

133   the two polymer species when present alone in THF solution. The formation and melting

134 temperatures of sPS and PEGDME gels in common and individual solution in THF were

135 determined by DSC, which provided the reference for the temperature around which the

136 detailed analysis of the conformational change between the simple coil and the regular form

137 of sPS as a function of solution composition was conducted.

138

139 **Experimental**

140 *Materials and sample preparation*

141 Syndiotactic polystyrene (sPS) (weight average molecular weight $M_W = 1.1 \times 10^5$ g/mol and

142 dispersity 1.9) was synthesized in both protonated (h-sPS) and deuterated (d-sPS) states

143 according to the coordination polymerization developed by [1], using styrene monomers with

144 a purity higher than 98% purchased from Cambridge Isotope Laboratories. PEGDME with

145 $M_W = 2 \times 10^4$ and 4×10^4 g/mol were synthesized in house in both protonated (h-PEGDME)

146 and deuterated (d-PEGDME) states using anionic polymerisation and characterized by size

147 exclusion chromatography [32]. Tetrahydrofuran (THF) was purchase in both protonated (h-

148 THF) and deuterated (d-THF) states from Sigma–Aldrich and used without further

149 purification.

150 For the study of gelation of sPS and PEGDME from common solution in THF and structure

151 and morphology analysis, the polymers were mixed in proper amounts in THF to obtain final

152 solutions with 5% sPS and 1% PEGDME v/v%, respectively. sPS and PEGDME were also

153 characterized separately in THF solutions. PEGDME of 20K and 40K were considered for

154 the structural study. For the gelation and melting analysis with DSC the solutions were

155 prepared for 5% sPS and 3% PEGDME v/v% in THF. sPS and PEGDME40K were also

156 investigated separately in THF solution. The small angle scattering of neutrons arises from

157 the fluctuations of the scattering length density (SLD) within the sample. For a ternary

158 system containing THF, sPS and PEGDME, the macroscopic cross-section can be expressed

159 in terms of the partial structure factors as

160

161 $d\Sigma/d\Omega(Q) = (\rho_{sPS} - \rho_{THF})^2 \, S_{sPS\text{-}sPS}(Q) + 2(\rho_{sPS} - \rho_{THF})(\rho_{PEGDME} - \rho_{THF}) \, S_{sPS\text{-}PEGDME}(Q)$ (1)

162 $+ (\rho_{PEGDME} - \rho_{THF})^2 \, S_{PEGDME\text{-}PEGDME}(Q)$

163

164 The partial scattering functions contain structural information about the sPS and PEGDME in

165 their solute or aggregated state and their mutual interaction. This information in principle

166 may be accessed separately by proper variation of the SLDs of the components in the ternary
167 system (Table 1) by D-labelling, thereby varying the contrast factors in Eq. 1. In order to
168 achieve the neutron contrast matching conditions between one polymer species and the
169 solvent in the initial solution and to keep the incoherent level at lowest level the following
170 combination schemes were used to specifically enable only one polymer species "visible"
171 while rendering the other one "invisible" in the SANS experiments: (i) h-sPS and d-
172 PEGDME in d-THF that enabled the sPS visible; (ii) d-sPS and h-PEGDME in d-THF for the
173 PEGDME visible; (iii) h-sPS and h-PEGDME in d-THF to have both polymers visible.

174

Sample	SLD [10^{-6} Å^{-2}]
h-PEGDME	0.64
d-PEGDME	6.90
h-sPS	1.40
d-sPS	6.42
h-THF	0.20
d-THF	6.35

175

176 The polymer solutions were prepared in tightly sealed sample cells made of bras and
177 equipped with ZnSe windows, allowing a beam path of 1 mm.

178

179

180

181 *Measurements*
182 For simultaneous SANS/FTIR measurements, an experimental setup combining a compact
183 portable FTIR spectrometer (Perkin-Elmer, Spectrum Two) and an optical system that plays
184 the role of beam mixer and selector was used. The optical system consists of a set of mirrors
185 that allows the extraction of the IR beam out of the spectrometer, enabling the coaxial
186 irradiation of sample by both the neutron and the IR beams, and the reflection of the scattered
187 IR beam back to the spectrometer, while enabling the scattered neutrons to arrive onto the
188 neutron detector placed a different distance from the sample. A detailed description of the
189 experimental setup can be found elsewhere [17].
190 During simultaneous SANS and FTIR experimental investigation the samples were heated in-
191 situ at about 110 °C (well above the boiling points of THF) and then cooled down to different

192 temperatures using an oil bath controlled from the SANS measurement software. SANS and

193 FTIR characterizations were carried out simultaneously at different gelation temperatures,

194 where a translucent gel was yielded. Empty sample container and solvent sample was

195 prepared and measured additionally.

196 The simultaneous SANS/FTIR measurements were carried at the BL15 beamline (the small

197 and wide-angle neutron diffractometer TAIKAN) at J-PARC, Tokai, Japan [33] and at the

198 KWS2 diffractometer of the Jülich Centre for Neutron Science (JCNS) at Heinz Maier-

199 Leibnitz Zentrum (MLZ), Garching, Germany [34]. At TAIKAN using the time-of-flight

200 method with a wide wavelength band (λ from 0.7 to 8 Å) a Q-range between 0.005 and 5 Å^{-1}

201 may be covered using the small-, middle- and wide-angle detectors. At KWS-2 the pinhole

202 SANS method with $\lambda = 5$ Å and neutron acquisition with the main detector placed at different

203 detection distances between 2 m and 20 m after the sample enables a Q-range between 0.001

204 and 0.6 Å^{-1}. Additional SANS measurements were carried out on selected samples and

205 conditions at KWS-2 using the pinhole mode with a longer wavelength $\lambda = 20$ Å and the

206 focussing mode with neutron lenses and a secondary high-resolution detector [35], which

207 enabled to reach the $Q_{min} = 2 \times 10^{-4}$ Å^{-1}.

208 The measured two-dimensional SANS data were subjected to typical corrections for the

209 empty cell contribution, instrumental background and detector sensitivity, calibrated in

210 absolute units of cm^{-1} by using the secondary standard sample of glassy carbon at TAIKAN

211 and of Plexiglas at KWS-2, and radially averaged to deliver the one-dimensional scattering

212 intensity I(Q).

213 Transmission IR spectra were taken simultaneously with SANS with a resolution of 2 cm^{-1} at

214 1 min intervals. For measuring the time dependence of IR spectra and analyzing them,

215 commercially available software (PerkinElmer, Timebase) was employed.

216 DSC characterizations of a h-sPS solution in h-THF and a common h-sPS and h-PEGDME

217 solution in h-THF were carried out using a differential scanning microcalorimeter Setaram

218 DSC131 EVO and samples sealed in stainless steel crucibles. The gels obtained by pre-

219 cooling homogeneous solutions in THF from 110 °C for sPS and mixed sPS-PEGDME and

220 from 50 °C for PEGDME were transferred to sample crucibles. Samples were heated to the

221 highest target temperature (110 °C if sPS was present, 50 °C otherwise) and DSC scans were

222 performed under a nitrogen atmosphere at a cooling/heating rate of 5 °C/min while samples

223 were cooled to the gel phase, followed by heating to observe the melting of the gel.
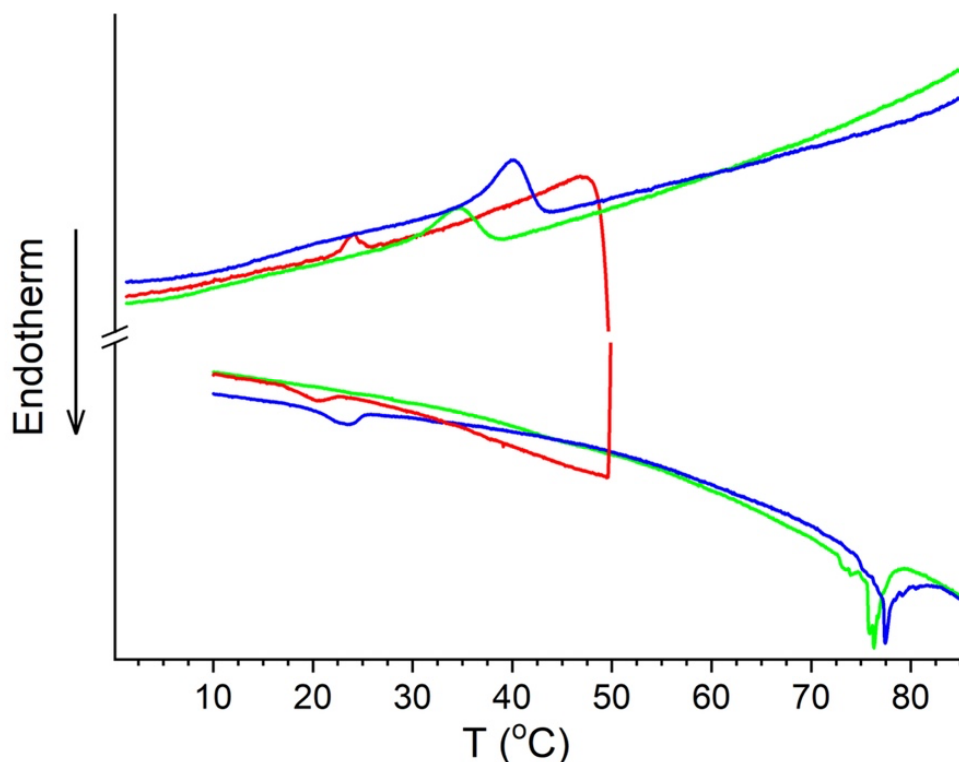
224

225

226 Figure 1 – Thermal behavior of the samples consisting of 5 % h-sPS and 3 % h-PEGDME40K in

227 common h-THF solution (blue line), 5 % h-sPS in h-THF solution (green line) and 3 % h-

228 PEGDME40K in h-THF solution (red line), determined by DSC during the melting and gelation

229 processes.

230

231

232 **Results**

233 The DSC thermograms with cycled cooling/heating procedure of the sPS and of

234 PEGDME40K individual solutions in THF and of sPS and PEGDME40K common solution

235 in THF for the polymers volume fraction in solution of ϕ_P = 5% and 3% for sPS and

236 PEGDME40K, respectively, are shown in Figure 1. Formation of sPS gel in THF occurs at

237 around T_c = 35 °C, while its melting takes place at higher temperatures over a broader range

238 between 70 °C and 80 °C. Gelation of h-PEGDME40K in THF appears at 25 °C, while the

239 melting at around 20 °C. The common solution of sPS and PEGDME40k in THF shows only

240 one gelation peak, at around T_c = 40 °C, while in melting two process can be observed: the

241 first one takes place at around 20 °C and can be assigned to melting of PEGDME40K gel,

242 while the second that appears over a broader range of higher temperatures, between 75 °C

243 and 85 °C, corresponds to the melting of sPS gel. The behavior of the sample containing

244 both polymers in common THF solution with only one gelation peak and two melting peaks

8

245 is characteristic of the co-assembly of the two polymer species, with the melting occurring at

246 the characteristic temperature T_m of each species, as observed for other systems too [36, 37].
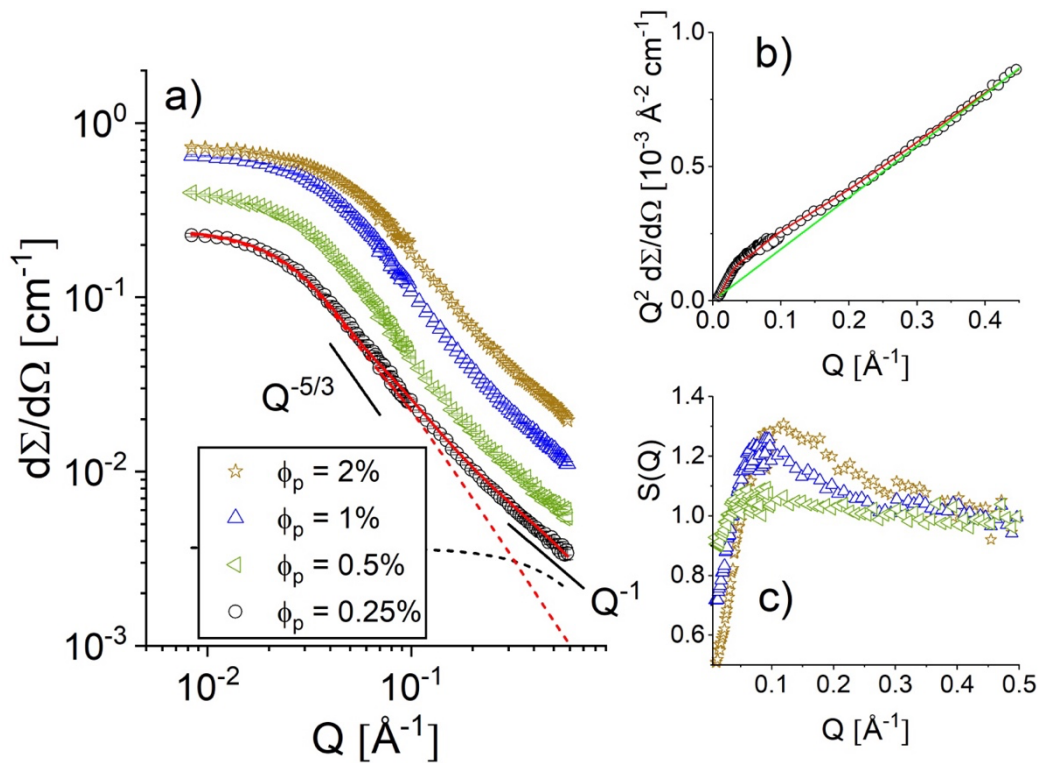
247

248
249

Figure 2 – Small angle scattering cross sections measured at 30 °C from a solution of h-PEGDME20k

251 in d-THF at different polymer volume fractions ϕ_p in solution, in a log-log presentation (a), the

252 Kratky-plot presentation of the scattering results obtained for $\phi_p = 0.25$ % (b) and the structure factor

253 that characterizes the scattering of highly concentrated samples (c). The solid black lines in panel (a)

254 show the power-law behavior of the scattering intensity in different Q-ranges, the solid red line

255 depicts the model interpretation of the data for the lowest polymer concentration, as described in the

256 text, while the dotted lines represent the contributions of the two structural levels considered in the

257 model. The solid red line in panel (b) has the same meaning as in panel (a), while the green line

258 indicates the signal from a rod-like morphology (see text).

259

260

261 Figure 2a shows the experimental SANS patterns measured on h-PEGDME20K solutions in

262 d-THF for different polymer volume fractions ϕ_P at 30 °C. For the most dilute sample ($\phi_P = $

263 0.25%) the power law exponents (Q^{-p}) specific for different morphologies of the polymer at

264 different length scales in solution are indicated. At small Q, where the Guinier region is

265 observed, the radius of gyration R_g of the polymer coil can be determined. At medium Q, a

266 characteristic decay exponent indicates the quality of the solvent: chains in a theta solvent

267 without interaction with excluded volume form Gaussian coils with a characteristic decay p =
268 2 of the scattering intensity, while chains with excluded volume in a good solvent, such as
269 PEO in THF [38], give an exponent p = 5/3. For semiflexible polymer chains, a transition to
270 Q^{-1} behavior follows at higher Q, whereby the polymer chain looks like a rod-like segment on
271 the length scale of the persistence length l_P. A polymer chain that gives rise to such scattering
272 features in SANS or SAXS can be described by the persistent wormlike chain model
273 established by Kratky and Porod [39]. Such polymer chains are characterized by long- and
274 short-range interactions and consist of average linear segments of a certain length, $l_K = 2 l_P$,
275 where l_K is the Kuhn step length, and a certain cross-sectional area A_K, i.e. the two-
276 dimensionally averaged, cross-sectional radius of gyration R_C orthogonal to the contour
277 length of the chain. l_K refers to the contour length L of the polymer chain by $L = n_K l_K$, where
278 n_K is the number of Kuhn units in the chain. A high molecular weight PEGDME chain in
279 dilute solution can therefore be treated with the Kratky-Porod model of a wormlike chain for
280 a persistent chain. Alternatively, it can be generally assumed that in a freely jointed chain,
281 rod-like segments of length l_K form a polymer chain of fractal mass dimension $d_f = 5/3$ or $d_f =$
282 2 for the polymer in good or theta solvent, respectively, as proposed by Beaucage [40]. The
283 interpretation of the scattering pattern for $\phi_P = 0.25\%$ using the proposed unified function
284 [41, 42] was done by considering the contribution of two structural levels, namely the overall
285 dimension (radius of gyration) of the coil and the substructural level l_P, as used in other
286 similar structural studies [43]. The unified equation applied to the two structural levels of a
287 persistent Kratky-Porod chain is given by:
288

$$I(Q) = \left\{ G_2 exp\left(-\frac{Q^2 R_{g2}^2}{3}\right) + B_2 exp\left(-\frac{Q^2 l_p^2}{3}\right)(q_2^*)^{-d_{f2}} \right\} +$$

289

$$\left\{ G_1 exp\left(-\frac{Q^2 R_{g1}^2}{3}\right) + B_1 exp\left(-\frac{Q^2 R_c^2}{3}\right)(q_1^*)^{-d_{f1}} \right\} \qquad (2)$$

290

291

292 where

$$q_n^* = \left[\frac{Q}{\{erf(1.06QR_g/\sqrt{6})\}^3} \right] \qquad (3)$$

293

294

295 for the two structural levels under consideration n = 1, 2.
296 The first bracket and the subscript "2" in Eq. 2 refer to the Guinier regime in the low Q range,
297 starting from the observed plateau and the bending of the scattering profile to high Q. The

298   second bracket and the subscript "1" describe the persistent rod-like scaling regime. The

299   fractal mass dimensions of the considered structural levels are described by the exponent df,

300   namely $d_f = 5/3$ or $d_f = 2$ for the polymer in good or theta solvent or $d_f = 1$ for the rod-like

301   morphology. A third term (the component "0") can be added to Eq. 2 if the scattering due to a

302   different local structural level is observed at very high Q values resulting from the cross-

303   sectional radius of persistence

304

305
$$\left\{ G_0 \exp\left(-\frac{Q^2 R_c^2}{3}\right) + B_0 (q_0^*)^{-4} \right\} \tag{4}$$

306

307   G_2 is the Guinier pre-factor ("forward-scattering") and R_{g2} is the radius of gyration

308   characterising the Guinier regime. For the persistent rodlike scaling regime $G_1 = G_2 / n_K$ and

309   R_{g1} is defined as

310

311
$$R_{g1} = \sqrt{\frac{l_P^2}{3} + \frac{R_c^2}{2}} \tag{5}$$

312

313   The pre-factor G_0 is defined as $G_0 = G_1 (R_c/(2l_P))^2$, as described in [41, 42]. Finally, the pre-

314   factors B_0 is the Porod pre-factor for a rod structure of length $2l_P$, while B_1 and B_2 relate to G_1

315   and R_{g1} and G_2 and R_{g2}, respectively, as described in [43] in details.

316   However, due to the limited Q range in our experiment, the length scale characteristic of the n

317   = 0 structure level could not be reached. Therefore, the experimental data were characterized

318   by the model described in Eq. 2. The red curve in Figure 2 shows the result of the model fit.

319   The contribution of the two structural levels considered is indicated by the dashed red and

320   black lines. The model interpretation of the experimental data yielded the most important

321   quantities for the structural characterisation of the high M_W PEGDME in THF, namely the

322   sizes $R_{g2} = 52.7$ Å and $l_P = 4.75$ Å as well as the forward scattering of the polymer in solution

323     $I_0 = G_2 = 0.245$ cm^{-1}. The "forward scattering" of an ensemble of protonated polymer coils

324   dissolved with a volume fraction ϕ_P in deuterated solvent is defined as $I_0 = \phi_P \Delta\rho^2 V_m$, where

325     $\Delta\rho$ is the neutron contrast representing the difference in SLD between the protonated polymer

326   and the deuterated solvent, and V_m is the molar volume of the polymer chain. The calculation

327   of the "forward scattering" from a volume fraction $\phi_P = 0.25\%$ of h-PEGDME20K in d-THF

328   considering the SLDs from Table 1 and a polymer mass density of 1.125 g cm^{-3} resulted in a

329   value of the "forward scattering" of $I_0^{calc} = 0.240$ cm^{-1}, which is very close to the measured

330   and fitted values. Figure 2b shows in a Kratky plot the scattering data of the lowest polymer

331   concentration in THF and the fit results according to Eq. 2 represented by the red curve. The

332   peculiarities of a Kratky-Porod chain can be clearly seen when compared with the feature of a

333   rod-like morphology, as indicated by the green line resulting from fitting the high Q portion

334   of the experimental results with a Q^{-1} power law.

335   As the volume fraction of the polymer in solution increases, correlation effects between the

336   polymer coils contribute to the scattering intensity, as shown in Figure 2c, as evidenced by

337   the structure factor S(Q). Typically, the scattering intensity of an ensemble of concentrated

338   scattering centers, such as polymer coils in solution, is expressed as $I(Q) = I_0\ P(Q)\ S(Q)$,

339   where P(Q) represents the form factor of the polymer coil, which reflects the intraparticle

340   correlations, while S(Q) represents the structure factor arising from the interparticle

341   correlations. At low ϕ_P, in the dilute regime, S(Q) = 1, while with increasing ϕ_P S(Q) starts to

342   become significant. S(Q) can be determined by dividing I(Q) measured for a high ϕ_P by the

343   intensity of the highly diluted particle ensemble, which is shown in Figure 2, considering that

344   S(Q) = 1 for ϕ_P = 0.25 %. For the highest volume fraction ϕ_P = 2 %, a correlation distance of

345   about 60 Å between the polymer coils can be estimated from the evaluation of the peak

346   position in S(Q).

347   The SANS scattering patterns of sPS and PEGDME20k individual solutions in d-THF at two

348   temperatures, 110 °C and 35 °C, above and just before the gelation point of the sPS in

349   solution are shown in Figure 3 in parallel with the SANS patterns of the two polymers in

350   common solution in d-THF, which were acquired for the contrast conditions that make each

351   of the polymer species "visible" during the measurement. The insert in Figure 3 shows the

352   same results in a Kratky plot. The results shown in Figure 3 were measured at the BL-15

353   Taikan beamline at J-PARC. The results from individual polymer solutions in d-THF are

354   shown by symbols in Figure 3. Both the sPS and the PEGDME20K are in coil form at 110

355   °C. The scattering characteristics typical of semiflexible coils are indicated by the power

356   laws, similar to Figure 2. The PEGDME20K result for ϕ_P = 1 % agrees very well with the

357   result reported in Figure 2, measured with the KWS-2 SANS diffractometer at 30 °C, and

358   thus shows a structure factor effect superimposed on the polymer form factor signal. It can be

359   assumed that the scattering pattern of the sPS is also influenced by correlation effects

360   between the polymer coils, although no detailed experimental analysis was performed on sPS

361   solutions with different ϕ_P. According to earlier SANS studies [23-25], sPS behaves like a

362 worm-like chain in benzene, toluene, chloroform or naphthalene-based solvents at high

363 temperatures.

364 At 35°C, the sPS alone in solution provides a strong scattering signal at low Q that deviates

365 significantly from single coil scattering. This indicates that some of the sPS chains have

366 assembled into an elongated, possibly fibrillar morphology, as indicated by the Q^{-1} power law

367 of intensity observed towards low Q, while most of the chains are still in the coil

368 conformation, as no noticeable decrease in intensity is observed at high Q. The formation of

369 the sPS-1D assemblies is driven by cooperative interactions between the sPS segments and

370 the solvent molecules as the gelation temperature of the polymer is approached. The Q^{-1}

371 power law behavior observed at low Q values indicates the formation of a fibrillar

372 morphology as reported in [23, 26], which may represent the junctions that promote the

373 formation of the polymer gel.

374

375
376
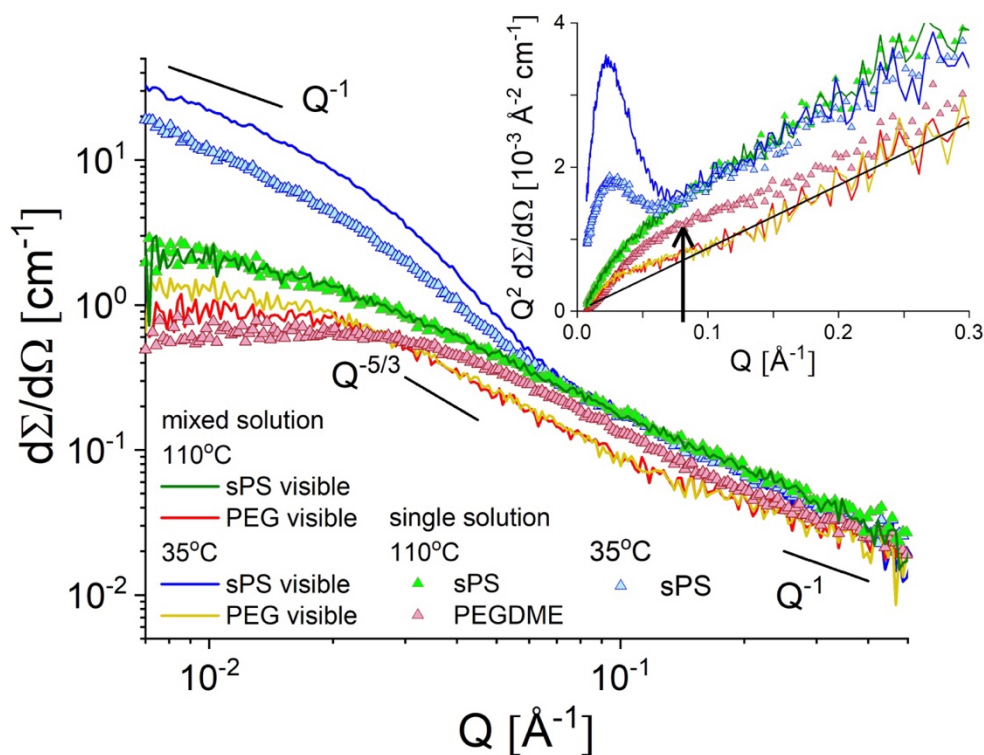
377 Figure 3 – Small angle scattering cross sections measured on sPS (ϕ_p = 5 %) and PEGDME20k (ϕ_p =

378 1 %) in common d-THF solution at decreasing temperature, from single coil conformation at 110 °C

379 to gelation of sPS at 35 °C, in parallel with the results obtained on individual polymer solutions in d-

380 THF. The sPS/PEGDME20K/d-THF ternary system was measured under different contrast conditions

381 that make one of the two polymer components visible, as indicated in the legend. The solid black lines

382 show the power law behavior of the scattering intensity in different Q-ranges. The inset shows the

383   same results in a Kratky-plot, with the black line representing the signal from a rod-like morphology

384   and the vertical arrow indicating the structure-factor effect for the PEGDME alone in solution.

385

386   The scattering of sPS from a joint solution with PEGDME20K in d-THF, measured at 110 °C

387   under a contrast condition that renders the PEGDME20K "invisible", agrees with the

388   scattering of sPS alone, indicating that the sPS is in single coil conformation at this

389   temperature. The contrast condition that makes PEGDME20K "visible" and sPS "invisible"

390   shows that the scattering pattern of PEGDME20K in single coil conformation is clearly

391   different from that of PEGDME20K in simple THF solution for the same $\phi_P = 1$ %: no

392   structure factor effect is observed and the scattering properties are similar to those of very

393   low ϕ_P in simple THF solution (Figure 2). Thus, the correlation effects between

394   PEGDME20K coils at $\phi_P = 1$ % disappear in the presence of the "invisible" sPS in solution,

395   and the scattering pattern only reveals the form factor of the PEGDME20K.

396   The Kratky plot of the results in the inset of Figure 3 clearly shows that the PEGDME20K

397   adopts a worm-like conformation in the joint THF solution with sPS at $\phi_P = 1$ %: For the

398   contrast condition visualizing the PEGDME20K, the same peculiarities are observed as for

399   the single polymer solution at the much lower polymer concentration in THF, shown in

400   Figure 2b. The effect of the structure factor characteristic of the single polymer solutions at

401   these high concentrations or affecting the sPS coils in the mixed solution, as evidenced by the

402   experimental results measured under the sPS contrast, is indicated by the vertical arrow in the

403   inset of Figure 3. These effects clearly lead to deviations from the scattering pattern

404   characteristic of a worm-like coil conformation.

405   A schematic representation of the conformation of the polymers in single and joint solution

406   for different scattering contrast conditions is suggested in the sketch in Figure 4.

407   The h-sPS/d-THF sample was additionally characterized on the KWS-2 diffractometer,

408   complemented by in situ FTIR, simultaneously with SANS. The SANS patterns are

409   consistent with those in Figure 3. The conformational range of the FTIR spectra recorded

410   simultaneously with SANS at two temperatures, 110 °C and 35 °C, is shown in Figure 5. The

411   spectra show the characteristic bands of sPS in amorphous coil form in solution at 110 °C

412   (538 cm^{-1}) and in helical TTGG conformation of the junctions in gel form at 35 °C (549 cm^{-1}

413   and 572 cm^{-1}). The configuration of the bands is similar to that reported in [22] in the study

414   of sPS gelation in chloroform, benzene and toluene. The right inset in Figure 5 shows the

415   time evolution of the band at 572 cm^{-1} after reaching the temperature of 35 °C on the sample

416   until its saturation, which shows that the gel is stabilized after about 15 minutes after reaching

417   the set temperature, which is information used at the beginning of the acquisition and analysis

418   of the SANS data. According to [44], gelation in SPS/o-dichlorobenzene and SPS/carbon

419   tetrachloride systems is completed within a few minutes at room temperature, whereas in

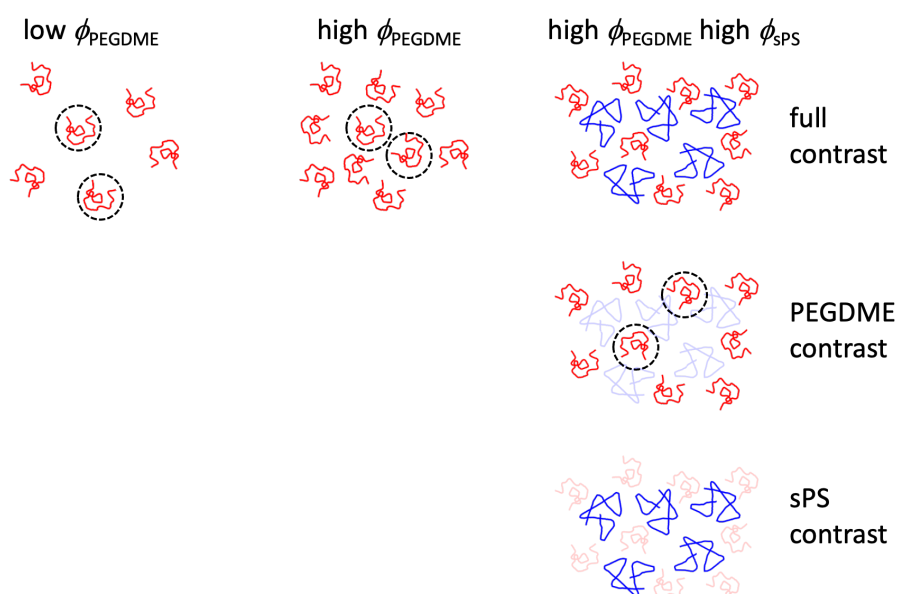420   SPS/chloroform it proceeds very slowly with a time scale of several tens of hours or longer.

421

422

423
424
425
426   Figure 4 – Cartoon depicting the proposed single chain arrangement of PEGDME in THF in the low

427   and high polymer concentration samples and the single chain arrangements of PEGDME and sPS as

428   revealed by the SANS contrast matching experiments. The correlation effects between the PEGDME

429   chains observed at high polymer concentration in THF alone were no longer observed when sPS was

430   added, as shown in the right column.

431

432

433   With all this information about the gelation/melting temperatures and the onset of gelation

434   associated with a conformational change of sPS between a single coil and a helix in

435   individual or joint polymer solutions, a detailed simultaneous SANS and in situ FTIR

436   characterization of sPS-PEGDME20K in a joint solution of d-THF was performed by

437   lowering the temperature from 110 °C to 20 °C, using the contrast matching for SANS.

438   Selected FTIR spectra at these two temperatures are shown in Figure 6, corresponding to the

439   different contrast conditions used in SANS. The region of the spectra corresponding to the

440   conformational bands of sPS (580 cm^{-1} to 520 cm^{-1}) shows essentially the same patterns as

441   those shown in Figure 5 for the contrast conditions that visualize sPS in the SANS

442 experiment (h-sPS). In the presence of PEGDME20K, the h-sPS bands corresponding to the

443 helical conformation at 20 °C are more pronounced, which is in good agreement with the

444 DSC observations showing that gelation occurs in the joint sPS and PEGDME20K solution in

445 THF at higher temperature than in the case of only sPS in THF (Figure 1).

446 The spectral region corresponding to the PEGDME conformational bands (1400 cm^{-1} to 1200

447 cm^{-1}), in which the characteristic bands of h-PEGDME should appear in amorphous (1352

448 cm^{-1}) and helical (1345 cm^{-1} and 1364 cm^{-1}) conformation [45], shows no qualitative change

449 with decreasing temperature down to 20 °C, indicating that the PEGDME20K does not adopt

450 a helical conformation below the gelation temperature of sPS. However, from the DSC

451 observations, we can already infer that although the PEGDME20K molecules do not form a

452 regular helical structure, segments of the long molecules can still adopt an elongated

453 conformation and that they are entrapped by the fibrillar sPS aggregates after a co-assembly

454 process with sPS driven by sPS gelation.
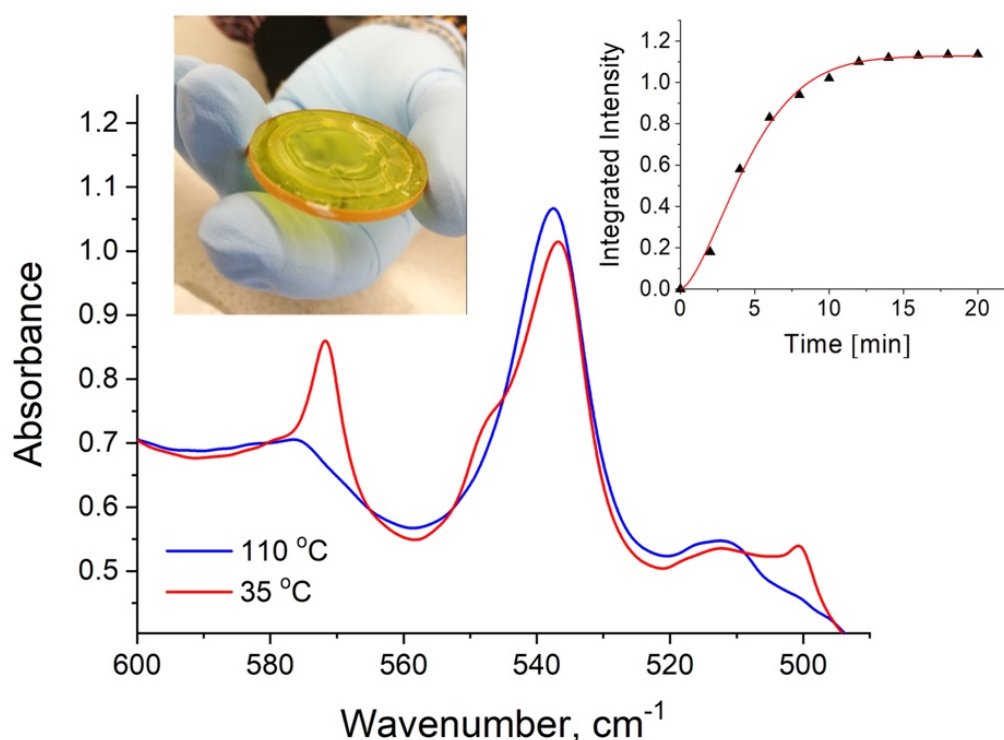
455

456

457
458
459 Figure 5 – IR spectra in the conformational band region of sPS in d-THF, measured at two

460 temperatures, above and at the gelation point observed by DSC (Figure 1). The FTIR measurements

461 were performed in-situ, simultaneously with the SANS experiment. The left inset shows the aspect of

462 the sample at the end of the experiment revealing the translucent polymer gel, while the right inset

463 shows the temporal evolution of the integrated intensity of the band developing at 572 cm^{-1}.

466   The SANS patterns shown in Figure 7 were recorded simultaneously with the FTIR analysis

467   under different contrast conditions that "visualize" either the sPS or the PEGDME20K. Both

468   polymers are in a single coil conformation at 110 °C, as can be seen from the form factor

469   scattering features. At 20 °C, the scattering features of polymer assemblies appear due to the

470   gelation process driven by sPS. According to DSC and FTIR observations, these are

471   structures formed jointly by sPS and PEGDME20K, with sPS adopting the crystalline helical

472   conformation and PEGDME20K having an amorphous elongated conformation.

473
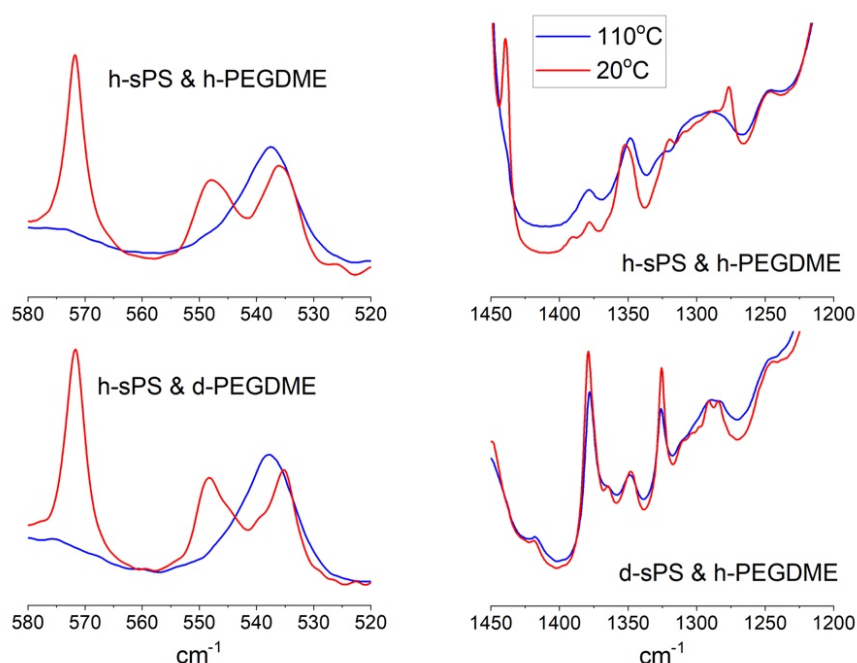
474
475   Figure 6 – Selected regions from the FTIR spectra measured at different temperatures simultaneously

476   with SANS on a common sPS and PEGDME20K solution in d-THF, for different neutron contrast

477   conditions, as indicated in the panels.

478

479

480   Two power laws can be recognized in the scattering patterns at medium and low Q ranges,

481   especially under sPS contrast conditions: The Q^{-2} power law observed in the medium Q range

482   turns into a Q^{-1} power law at low Q values, indicating the formation of elongated structures

483   with a 1D overall aspect that exhibit a 2D aspect on a smaller length scale corresponding to

484   the lateral size of the aggregates. Fibrillar or platelet-like morphologies result in such a

scattering pattern. These polymer aggregates are mainly composed of helical sPS with
elongated PEGDME20K segments sandwiched between sPS helices, which are the junctions
of the polymer gel. Therefore, both sPS and PEGDME20K should have long segments that
are still amorphous and extend away from the aggregating objects, resulting in the network-
like character of the gel. At high Q, the power-law behavior of the scattering intensity for
both contrast conditions suggests a single coil form factor, which could correspond to the
larger coils still in solution and the smaller amorphous segments extending away from the
polymer aggregates.
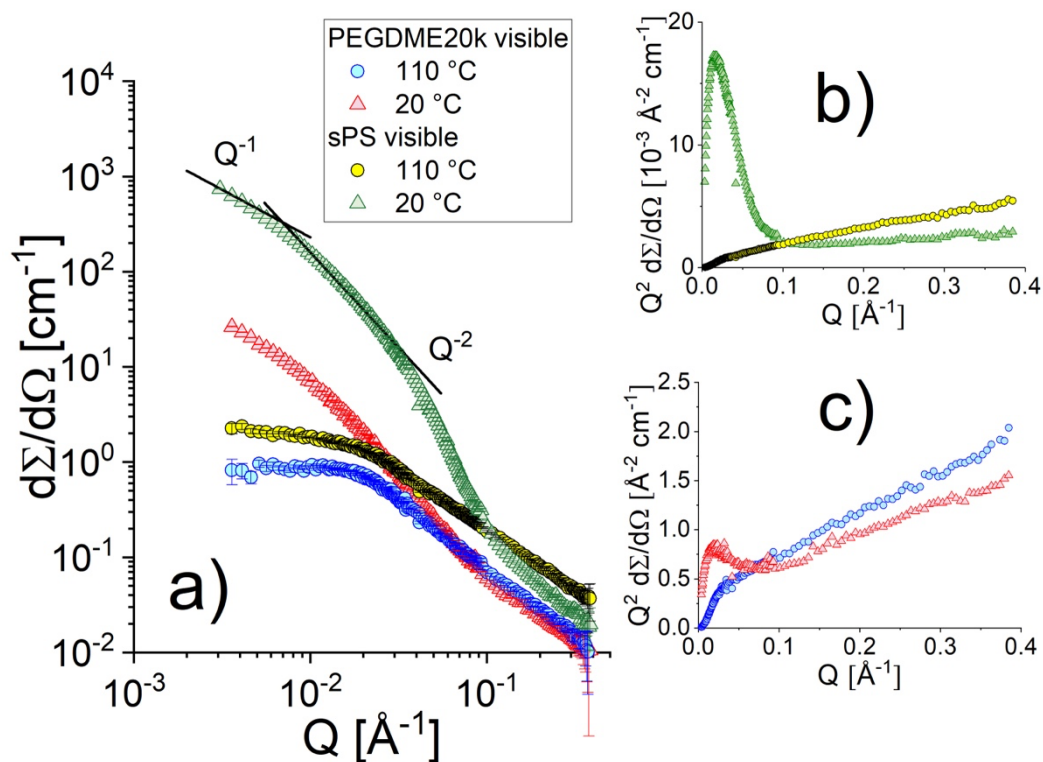
Figure 7 – Small angle scattering cross sections measured under different contrast conditions of sPS
(ϕ_P = 5 %) and PEGDME20k (ϕ_P = 1 %) mixed in common d-THF solution at decreasing temperature
from the single coil conformation regime at 110 °C to the gelation regime of sPS at 20 °C shown in
log-log representation (a) and in as Kratky plots (b, c). The contrast conditions visualize always one
of the two polymer components as indicated in the legend. The solid black lines show the power law
behavior of the scattering intensity in different Q-ranges.

506   On the other hand, the fact that in the sPS contrast condition at low temperatures, the

507   intensity at high Q decreases compared to the intensity at 110 °C suggests that a large number

508   of sPS chains are already incorporated into the aggregates in spiral conformation, reducing

509   the volume fraction of the sample occupied by the polymer still in coil form. The observation

510   that both patterns follow the same qualitative behavior under sPS and PEGDME20K contrast

511   conditions, differing only in intensity (which is much higher in the case of the "visible" sPS),

512   suggests that sPS and PEGDME20K are uniformly distributed in the aggregates formed by

513   association involving both polymer species. Since the contrast between the two polymer

514   species in hydrogenated form and the deuterated THF is quite similar (Table 1), the

515   difference in intensity can be attributed to the different volume fraction of the two polymer

516   species within the aggregates. Assuming a homogeneous distribution of the two types of

517   polymer molecules within the aggregates and also the compact aggregates, then

518

519    $$I(Q) \approx \phi_{agg}\Delta\rho_{agg}^2 = \Phi_{agg}\left(\phi_{sPS}^{agg}\Delta\rho_{sPS}^{agg} + \phi_{PEGDME}^{agg}\Delta\rho_{PEGDME}^{agg}\right)^2 \qquad (6)$$

520

521   with ϕ_{agg} - the volume fraction of the sample occupied by the aggregates, $\Delta\rho_{agg}$ - the contrast

522   between the aggregates and their surroundings, and the factors on the right-hand side of the

523   equation within the paranthesis, which represent the volume fraction of an aggregate

524   occupied by one of the two polymer species, multiplied by the corresponding contrast factor

525   squared. Thus, for each contrast condition, one of the two terms on the right-hand side within

526   the paranthesis disappears, so that the measured intensity is proportional to the volume

527   fraction of the "visible" polymer species within the aggregate. A rough estimate of the

528   intensity at Q_{min} for each of the contrast conditions in Figure 7 shows that the volume fraction

529   of the aggregate occupied by sPS is about five times larger than that of PEGDME20K, which

530   corresponds to the ratio between the two volume fractions of the polymers in the original

531   joint solution. The co-assembly process thus leads to a homogeneous distribution of the two

532   polymers within the aggregates.

533   The results of the SANS measurements performed on a joint sPS and PEGDME40K solution

534   in THF at decreasing temperature between the single coil mode at 110 °C and the co-

535   assembly regime at 10 °C are shown in Figure 8. The Q range was extended to lower Q

536   values compared to the previous SANS analyses. The same type of scattering features were

537   observed as in the case of PEGDME20K. At very low Q values, a tendency towards an

538 increase in intensity with respect to the Q^{-1} behavior can be assumed (vertical arrow mark),

539 which could be related to the scattering from the large-scale network-like gel morphology.

540 In an early SANS study on physical gels formed by sPS in $CDCl_3$, the data were interpreted

541 using a model combining mass and surface fractal features with the approach of Guinier and
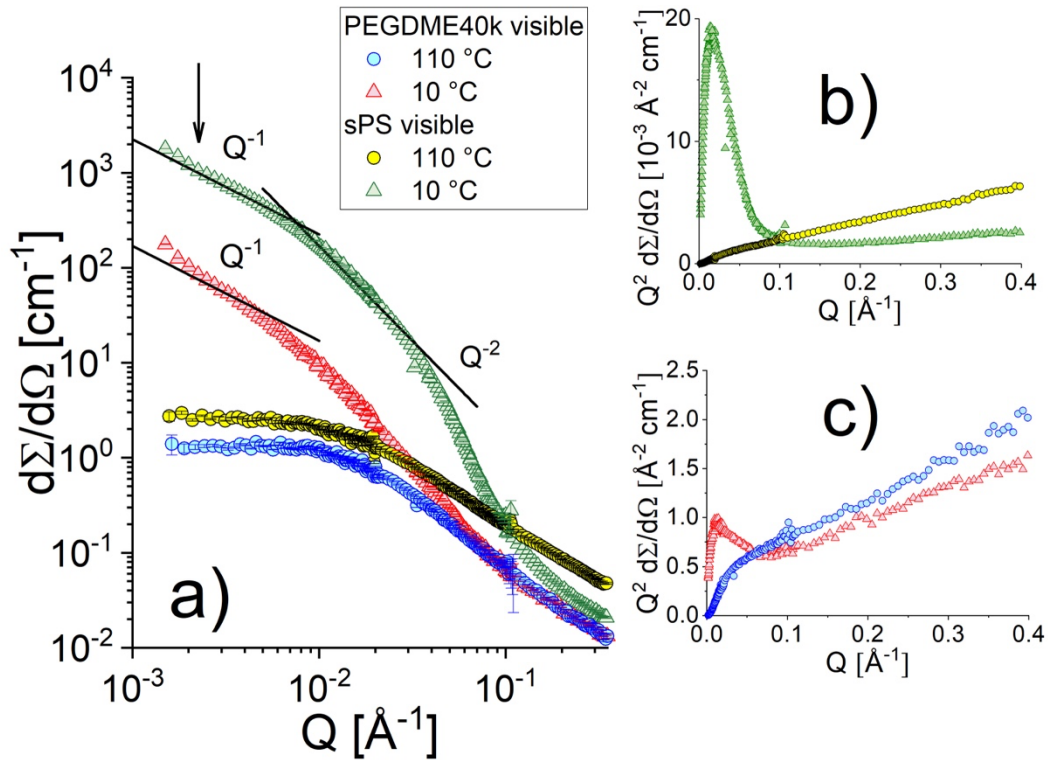
542 Kratky plots [46].

543
544
545 Figure 8 – Small angle scattering cross sections measured under different contrast conditions of sPS

546 (ϕ_P = 5 %) and PEGDME40k (ϕ_P = 1 %) mixed in common d-THF solution at decreasing temperature

547 from the single coil conformation at 110 °C to the gelation state of sPS at 10 °C; panels a, b, c and

548 lines and symbols with the same meaning as in Figure 7.

549

550

551 Motivated by the observation of the scattering features in the SANS patterns measured in the

552 gel state, namely the observed Q^{-2} power law at medium Q, indicative of the 2D aspect of the

553 aggregates at the lower size scale, and the Q^{-1} power law at low Q, characteristic of the

554 overall 1D aspect of the aggregates at the larger length scale, for the simultaneous

555 interpretation of the scattering data measured at 10 °C for the three contrast conditions (sPS

556 visible, PEGDME40K visible and both polymers visible), a model combining the form factor

557 of a long parallelepipedon [47] with the coil form factor at high Q values and a Q^{-3} power law

558 in the very low Q range was used. The parallelepipedon form results in the Q^{-2} power law

559 behavior of the scattering pattern at medium Q values, which changes to a Q^{-1} behavior

towards lower Q values. The length of such one-dimensional aggregates in the overall aspect and the transition to the network generated by such cross-linking structures can be estimated from the Q value, where the increase in intensity occurs at very low Q and deviates from the Q^{-1} behavior. The coil shape factor represents the scattering contribution at high Q, while the steeper power law at low Q comes from the contribution of gel morphology with larger length scale, most of which scatters outside the Q range covered in this experiment.
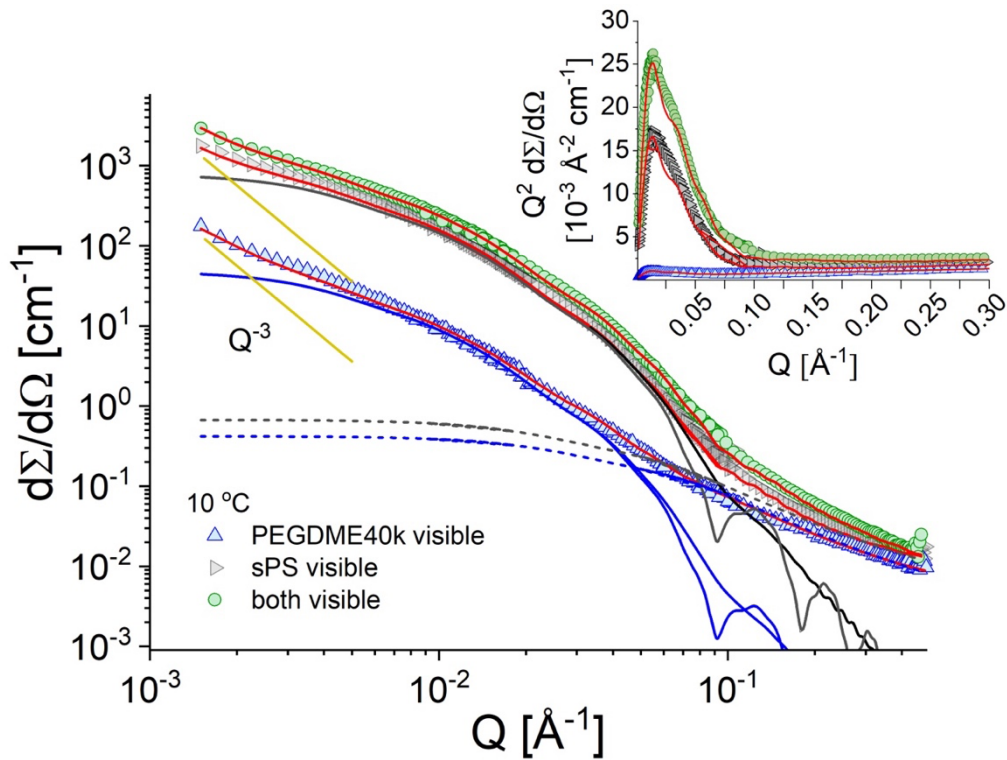
Figure 9 – Model interpretation of the SANS patterns of the aggregates formed by gelation of sPS and PEGDME40K in common solution in d-THF at 10 °C shown in log-log (main plot) and Kratky (inset plot) representations: the symbols are experimental data measured under different contrast conditions, as explained in the legend, while the red curves represent the results of simultaneous fitting of all three SANS patterns, as described in the text; the black and blue solid lines represent the scattering contribution of the aggregates, while the dashed lines show the scattering contribution of the polymer coils; the additional contribution of the large-scale gel network is shown as a power law at low Q.

The parallelepipedon model that assumes a rectangular cross section and an elongated aspect was developed in [47]:

21

581

$$I(Q) =$$

$$I_0 \frac{(l_a l_b l_c)^2}{4\pi} \int_0^{2\pi} \int_0^{\pi} \left[\frac{\sin(\pi Q l_a \sin\varphi \cos\psi)}{\pi Q l_a \sin\varphi \cos\psi}\right] \left[\frac{\sin(\pi Q l_b \sin\varphi \sin\psi)}{\pi Q l_b \sin\varphi \sin\psi}\right] \left[\frac{\sin(\pi Q l_c \cos\varphi)}{\pi Q l_c \cos\varphi}\right] \sin\varphi \, d\varphi \, d\psi \qquad (7)$$

where I_0 is the forward scattering, which takes into account the contrast factor squared to the volume fraction of the scattering objects, l_a, l_b and l_c are the side lengths of the parallelepipedon, and φ and ψ are the polar and the azimuthal angles, respectively. Additional scattering contributions from the coils of the two polymers connecting the gel compounds or still in solution and the large-scale gel structure at high Q or low Q were added to Eq. 7. To simplify the model, the contribution from the coils was modelled using the unified equation (Eq. 2) for only one structural level with the exponent 5/3 and the main fitting parameters I_0coil and $R_g$coil, while the contribution from the gel at low Q was interpreted as $P_3 Q^{-3}$, with the P_3 pre-factor as the fitting parameter.

Table 2 – Parameters delivered by the fitting procedure of the experimental data at 10 °C according to the model discussed in the text.

contrast condition / parameter	sPS visible	PEGDME40K visible
I_0 aggregates [cm^{-1}]	563.40 ± 22.35	28.59 ± 1.90
l_a, thickness [Å]	35.22 ± 0.99	35.22 ± 0.99
l_b, width [Å]	140.72 ± 3.55	140.72 ± 3.55
l_c, length [Å]	591.10 ± 22.34	591.10 ± 22.34
I_0coil [cm^{-1}]	0.34 ± 0.07	0.21 ± 0.04
$R_g$coil [Å]	62.60 ± 7.80	54.1 ± 6.90
P_3 [cm^{-1} Å^{-3}]	2.10E-6	2.5E-7

The results of the fitting procedure applied to the data measured at 10 °C simultaneously for all contrast conditions are shown as lines in Figure 9. The red lines indicate the global fitting results, while the blue and black solid lines represent the contribution of polymer aggregates for the visible PEGDME40K and sPS, respectively. The fitting procedure provided the three

604   dimensions of the aggregates, l_a - the thickness, l_b - the width and l_c - the length, and the

605   forward scattering I_0, which depends on the SLD of the aggregates for the different contrast

606   conditions considered, i.e. the volume fraction of the aggregate occupied by each polymer

607   species. In addition, the R_g value of the polymer coils and their forward scattering were

608   determined for each polymer species under the corresponding contrast conditions, as well as

609   the pre-factor P_3 of the Q^{-3} power law at low Q value. Due to the good separation of the fitted

610   morphologies on the length scale, the parameters determined by the model interpretation

611   method are quite reliable. The structure and specific scattering parameters resulting from the

612   fitting are listed in Table 2. The analysis of the "forward scattering" of the aggregates

613   according to Eq. 2 shows that the fibrillar, board-like morphologies consist of approx. 83%

614   sPS and 17% PEGDME40K, which roughly corresponds to the ratio of the concentrations of

615   the two polymer species in the initial solution in THF. Thus, it can be assumed that segments

616   of the PEGDME polymer are incorporated into the aggregated structure driven by the sPS

617   gelation with the solvent molecules, and the fact that no PEGDME crystallization was

618   observed suggests that the PEGDME segments are located between the sPS helices rather

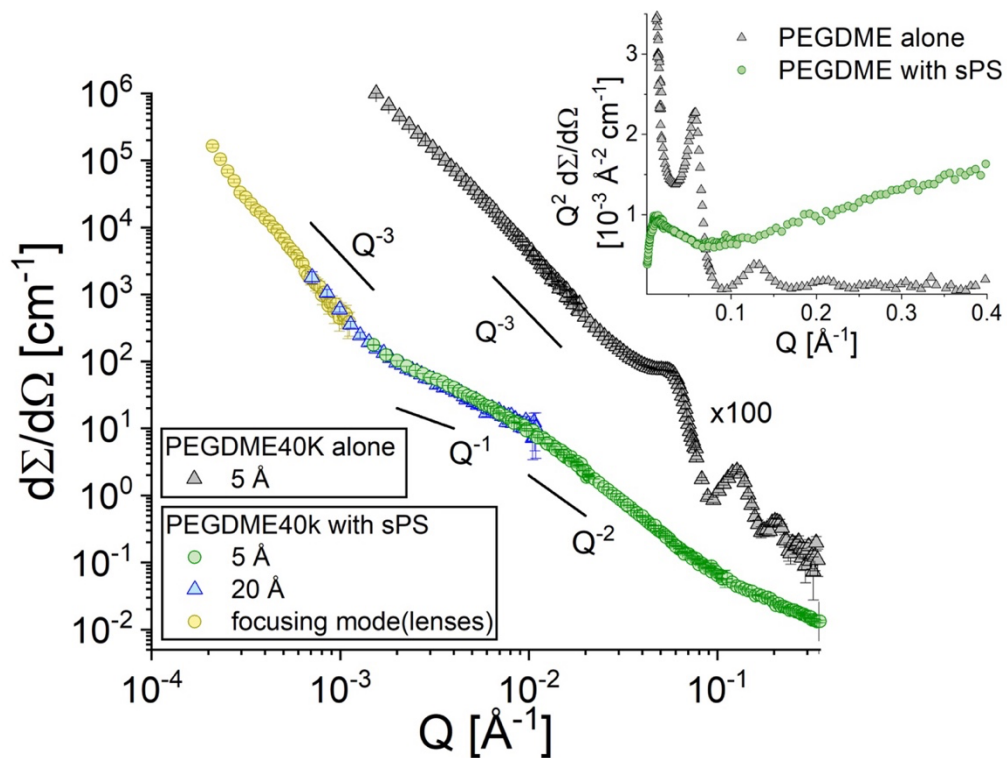619   than forming well-defined domains within the aggregates.

620

621

622
623
624

625   Figure 10 – SANS patterns of h-PEGDME40K morphology formed in d-THF (ϕ_{pol} = 3 %) collected at

626   10 °C (black symbols), in parallel with the scattering contribution of h-PEGDME40K (ϕ_{pol} = 1 %)

627   (green/blue/yellow symbols), when co-assembled with d-sPS in common solution in d-THF

628   (scattering from d-sPS was matched-out). The power law behavior of the scattering intensity in

629   different Q-ranges is indicated as explained in the text. The inset shows the results measured over the

630   conventional SANS-Q range in a Kratky plot.

631

632

633   The inset in Figure 9 shows the experimental data and the overall results of the fit for all three

634   contrast conditions considered in a Kratky plot. The model describes the scattering features

635   shown in this plot quite well, although some discrepancies can be observed around Q = 0.03

636    $Å^{-1}$. However, considering that the model is a rough approximation of a real morphology that

637   should be characterized by smearing factors of all side lengths specific to all contrast

638   conditions, we can assume that the interpretation of the scattering data by the

639   parallelepipedon model generally describes all observed features and the cooperative gelation

640   of the two types of polymers quite well. The sPS effect on the behavior of PEGDME with

641   high MW is evident by comparing the scattering pattern of PEGDME40K (ϕ_{pol} = 1 %) co-

642   assembled with sPS in common aggregates from THF solution with the scattering pattern of

643   PEGDME40K alone (ϕ_{pol} = 3 %) in THF at 10 °C, as shown in Figure 10. PEGDME alone

644   forms a "house of cards" gel in THF, as indicated by the Q^{-3} power law behavior at medium

645   Q, which consists of stacked lamellar structures at smaller length scale, as evidenced by the

646   interlamellar correlation peak and higher order correlations at smaller length scale, as

647   indicated by the scattering features observed at high Q. In the presence of sPS, smaller and

648   softer structures appear, with the PEGDME molecules involved in the formation of fibrillar

649   morphologies with a localized 2D aspect as a result of a cooperative gelation process

650   controlled by sPS. These morphologies represent the junctions of a gel network that scatters

651   at much lower Q values, as shown in Figure 10. Using pinhole and focusing SANS data

652   collected over a wide Q range, the contribution of PEGDME to scattering from the large-

653   scale gel structure at very low Q values can be recognized.

654

655

656   **Conclusions**

657   Physical gelation of sPS in the presence of high M_W PEGDME from THF solution was

658   studied by contrast variation SANS. Contrast matching was used to characterize the

scattering contribution of each component in the ternary system and to follow the behavior of each polymer species during gelation process. The gelation and melting temperatures of mixed and individual polymer solutions in THF were determined by DSC. The formation and evolution of the structure and morphology at different gelation temperatures in transition from the single-coil conformation of the two polymer species at 110 °C to the ordered regular conformational of sPS in gel phase was additionally monitored in-situ by FTIR analysis of the samples simultaneously with SANS. A cooperative gelation process of sPS and high M_W PEGDME was observed. sPS changes from the amorphous coil to the helical TTGG conformation when the gelation temperature is passed, forming fibrillar morphologies with a local 2D aspect, as revealed by the scattering data, due to cooperative interactions with the solvent molecules. These aggregates are the junction structures of the large-scale network morphology of the gel. The high molecular weight PEGDME transitions from the amorphous coil to an elongated amorphous conformation and incorporates into the fibrillar morphology together with the sPS during the gelation process. High M_W PEGDME alone in THF forms a "house of cards" gel consisting of stacked lamellar structures on a smaller length scale, as shown by the scattering data. Thus, in the presence of sPS, smaller and softer structures appear as a result of a cooperative gelation process controlled by sPS. According to other structural studies, the structure of sPS fibrils in gel form is identical to the structure of the co-crystalline phase of sPS δ (clathrates and intercalates). The incorporation of high M_W PEGDME into these aggregates thus leads to polymer nanocomposites that can render the sPS hydrophilic, a topic that should be the focus of future structural and morphological studies.

References

[1] N. Ishihara, T. Seimiya, M. Kuramoto, M. Uoi, Macromolecules 1986, 19, 2464-2465.

[2] G. Guerra, V.M. Vitagliano, C. DeRosa, V. Petraccone, P. Corradini, Macromolecules 1990, 23, 1539-1544.

[3] Y. Chatani, Y. Shimane, Y. Inoue, T. Inagaki, T. Ishioka, T. Ijitsu, T. Yukinari, Polymer 1992, 33, 488-492.

[4] E. Bhoje Gowd, K. Tashiro, C. Ramesh, Prog. Polym. Sci. 2009, 34, 280-315.

[5] O. Tarallo, M.M. Schiavone, V. Petraccone, C. Daniel, P. Rizzo, G. Guerra, Macromolecules 2010, 43, 1455-1466.

[6] O. Tarallo, M.M. Schiavone, V. Petraccone, Eur. Polym. J. 2010, 46, 456-464.

[7] O. Tarallo, M.M. Schiavone, V. Petraccone, Polymer 2011, 52, 1426-1435.

[8] Y. Uda, F. Kaneko, T. Kawaguchi, Polymer 2004, 45, 2221-2229.

[9] Y. Uda, F. Kaneko, T. Kawaguchi, Macromolecules 2005, 38, 3380-3385.

[10] P. Rizzo, S. Della Guardia, G. Guerra, Macromolecules 2004, 37, 8043-8049.

[11] C. Daniel, A.R. Albunia, C. D'Aniello, P. Rizzo, V. Venditto, G. Guerra, Journal of the European Optical Society - Rapid Publications 2009, 4, 09037.

[12] P. Stegmaier, A. De Girolamo Del Mauro, V. Venditto, G. Guerra, Adv. Mater. 2005, 17, 1166-1168.

[13] M. Giordano, M. Russo, A. Cusano, G. Mensitieri, G. Guerra, Sensors and Actuators B 2005, 109, 177–184.

[14] P. Rizzo, C. Daniel, G. Guerra, Macromolecules 2010, 43, 1882-1887.

[15] G. Milano, G. Guerra, Prog. Mater. Sci. 2009, 54, 68-88.

[16] F. Kaneko, K. Sasaki, Macromol. Rapid Comm 2011, 32, 988-993.

[17] F. Kaneko, N. Seto, S. Sato, A. Radulescu, M.M. Schiavone, J. Allgaier, K. Ute, Chem. Lett. 2015, 44, 497–499.

[18] S. Sato, T. Kawaguchi, F. Kaneko, Macromol. Symp. 2016, 369, 114-118.

[19] S. Sato, Y. Yamamoto, F. Kaneko, Chem. Lett. 2019, 48, 177–180.

[20] F. Kaneko, N. Seto, S. Sato, A. Radulescu, M. M. Schiavone, J. Allgaier, K. Ute, J. Appl. Crystallogr. 2016, 49, 1420-1427.

[21] H. Shimizu, T. Wakayame, R. Wada, M. Okabe, F. Tanaka, Polym. J. 2005, 37, 294-298.

[22] M. Kobayashi, T. Yoshioka, M. Imai, Y. Itoh, Macromolecules 1995, 28, 7376-7385.

726   [23] C. Daniel, M. D. Deluca, J-M. Guenet, A. Brulet, A. Menelle, Polymer 1996, 37, 1273-

727   1280.

728   [24] C. Daniel, A. Menelle, A. Brullet, J-M. Guenet, Polymer 1997, 38, 4193-4199.

729   [25] S. Malik, C. Rochas, M. Schmutz, J-M. Guenet, Macromolecules 2005, 38, 6024-6030.

730   [26] C. Daniel, S. Giudice, G. Guerra, Chem. Mater. 2009, 21, 1028-1034.

731   [27] C. Daniel, G. Guerra, P. Musto , Macromolecules 2002 , 35 , 2243-2251.

732   [28] J. Mochizuki, T. Sano, T. Tokami, H. Itagaki, Polymer 2015, 67, 118-127.

733   [29] K. Senoo, S. Matsuda, S. Kohjiya, e-Journal of Soft Materials 2006, 2, 31–36.

734   [30] X. Wang, S. C. Jana, Langmuir 2013, 29, 5589−5598.

735   [31] B. Hammouda, D. L. Ho, S. Kline, Macromolecules 2004, 37, 6932-6937.

736   [32] C.H. Hövelmann, S. Gooßen, J. Allgaier. Macromolecules 2017, 50, 4169–4179

737   [33] S. Takata, J. Suzuki, T. Shinohara, T. Oku, T. Tominaga, K. Ohishi, H. Iwase, T.

738   Nakatani, Y. Inamura, T. Ito, JPS Conf. Proc. 2015, 8, 036020.

739   [34] A. Radulescu, V. Pipich, H. Frielinghaus, M.S. Appavou, Journal of Physics Conference

740   Series 2012, 351, 012026.

741   [35] A. Radulescu, N.K. Szekely, M.S. Appavou, V. Pipich, T. Kohnke, V. Ossovyi, S.

742   Staringer, G.J. Schneider, M. Amann, B. Zhank-Haagen, G. Brandl, M. Drochner, R. Engels,

743   R. Hanslik, G. Kemmerling, J. Vis. Exp. 2016, 118, e54639.

744   [36] Y. Qu, L. Li, G. Lu, X. Zhou, Q. Su, W. Xu, S. Li, J. Zhang, X. Yang., Polym. Chem.

745   2012, 3, 3301-3307.

746   [37] P. Shaiju, N. Sanjeeva Murthy, E. Bhoje Gowd, Macromolecules 2016, 49, 224−233.

747   [38] S. H. Nguyen, D. Berek, I. Capek, O. Chiantore, Journal of Polymer Science: Part A:

748   Polymer Chemistry 2000, 38, 2284–2291.

749   [39] O. Kratky.; G. Porod, Rec. Trav. Chim. Pays-Bas 1949, 68, 1106-1122.

750   [40] G. Beuacage, S. Rane, S. Sukumaran, M.M. Satkowski, L.A. Schechtman,

751   Macromolecules 1997, 30, 4158-4162.

752   [41] G. Beaucage, J. Appl. Cryst. 1995, 28, 717-728.

753   [42] B. Hammouda, J. Appl. Cryst. 2010, 43, 1474-1478.

754   [43] R. Ramachandran, G. Beaucage, A. S. Kulkarni, D. McFaddin, J. Merrick-Mack, V.
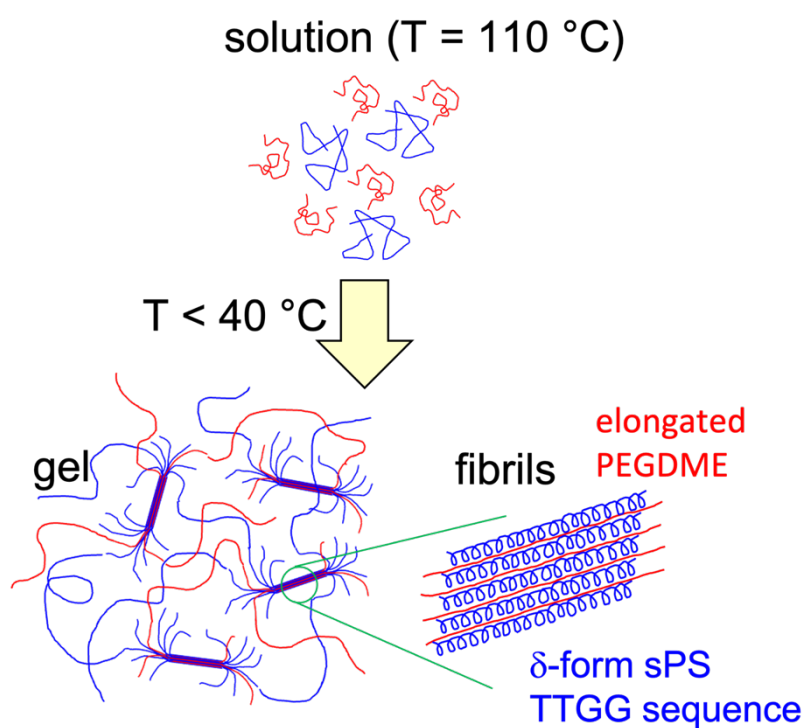
755   Galiatsos, Macromolecules 2008, 41, 9802-9806.

756   [44] M. Kobayashi, T. Yoshioka, M. Imai, Y. Itoh, Physica B, 1995, 213&214, 734-736

757   [45] M. Kobayashi, K. Kitagawa, Macromol. Symp. 1997, 114, 291-296.

758   [46] M. Kobayashi, T. Yoshioka, T. Kozasa, K. Tashiro, J. Suzuki, S. Funahashi,

759   Y. Izumi, Macromolecules 1994, 27, 1349-1354.

760 [47] J. S. Pedersen, Adv. Colloid Interface Sci. 1970, 70, 171-210.

761

762

763

764

765

766

767

768

769

770

771

772

773

774

775

776

777

778   Graphical Abstract:

779

780

781

782